Talanta 87 (2011) 15–23

Contents lists available at SciVerse ScienceDirect

Talanta

journal homepage: www.elsevier.com/locate/talanta

Preparation and characterization of bismuth oxide nanoparticles-multiwalled carbon nanotube composite for the development of horseradish peroxidase based H_2O_2 biosensor

Arun Prakash Periasamy, Singying Yang, Shen-Ming Chen*

Department of Chemical Engineering and Biotechnology, National Taipei University of Technology, No. 1, Section 3, Chung-Hsiao East Road, Taipei 106, Taiwan, ROC

ARTICLE INFO

Article history:
Received 24 July 2011
Received in revised form
12 September 2011
Accepted 13 September 2011
Available online 5 October 2011

Keywords:
Direct electrochemistry
Horseradish peroxidase
Bi_2O_3
Multiwalled carbon nanotubes
Electrocatalysis
Hydrogen peroxide

ABSTRACT

In this work, preparation and characterization of a novel nanocomposite containing bismuth oxide (Bi_2O_3) nanoparticles and multiwalled carbon nanotubes (MWCNTs) was presented. Powder X-ray diffraction (XRD) studies revealed that as-synthesized Bi_2O_3 nanoparticles are crystalline and belong to α-phase with monoclinic symmetry. Field emission scanning electron microscopy (FESEM) study results showed that the size of Bi_2O_3 nanoparticles is 50 nm. Energy-dispersive X-ray (EDX) spectra of as-prepared Bi_2O_3–MWCNT nanocomposite displayed characteristic Bi and C peaks which confirmed the incorporation of Bi_2O_3 with MWCNT. The prepared Bi_2O_3–MWCNT was also characterized by scanning electron microscopy (SEM) and atomic force microscopy (AFM) studies. The direct electron transfer of horseradish peroxidase (HRP) has been revealed at Bi_2O_3–MWCNT modified glassy carbon electrode (GCE). In order to firmly anchor the HRP molecules onto Bi_2O_3–MWCNT matrix, a thin layer of 1% nafion (NF) solution was coated as a binder. The fabricated NF/HRP/Bi_2O_3–MWCNT/GCE exhibits well defined quasi-reversible redox peaks at a formal potential ($E^{0\prime}$) of −0.326 V vs. Ag/AgCl reference electrode in 0.05 M phosphate buffer solution (PBS), pH 7. NF/HRP/Bi_2O_3–MWCNT film remarkably lowers the over potential for H_2O_2 reduction than MWCNT, Bi_2O_3–MWCNT and unmodified GCEs. The proposed composite film exhibits quick amperometric *i*–*t* response (5 s) towards H_2O_2 in the linear range of 8.34–28.88 mM with a sensitivity of 26.54 μA μM^{-1} cm^{-2}. The developed NF/HRP/Bi_2O_3–MWCNT biosensor has a good operational stability and high selectivity towards H_2O_2.

1. Introduction

In recent years, owing to the large surface area, high mechanical resistance, and high electronic conductivity [1], multiwalled carbon nanotubes (MWCNTs) and their composites have been extensively used for biosensors [2], fuel cells [3], solar cells [4] and photovoltaics [5] applications. MWCNT composites with metal nanoparticles [6], metal oxide nanoparticles [7], and conducting polymers [8,9] have been widely employed for the sensitive and selective determination of essential compounds such as ascorbic acid, epinephrine, uric acid, catechol and quinol. Since, metal oxides possess unique advantages such as high sensitivity, good selectivity and large surface-to-volume ratio, so far increasing number of researchers have reported the production of novel CNT–metal oxide nanocomposites for biosensors applications [10,11]. MWCNT–metal oxide composites have also been employed in supercapacitors [12], electrochemical capacitors [13], and lithium ion batteries [14].

Bismuth oxide (Bi_2O_3) is a well known transition metal oxide and it has been intensively studied due to its interesting thermal and electrical transport properties [15]. Moreover, Bi_2O_3 nanoparticles can offer large surface area and good electrochemical stability. Recently Bi_2O_3 nanoparticles have attracted considerable attention due to their potential applications in electrochemical sensors for sensing zinc [16], paracetamol [17] and to probe DNA hybridization [18]. Owing to its unique properties such as nontoxic nature, excellent chemical inertness and biocompatibility, it has been employed as potential immobilizing platforms for glucose oxidase [19], and polyphenol oxidase [20].

Hydrogen peroxide (H_2O_2) has received considerable attention because of its good antiseptic and antibacterial property [21]. Due to its excellent oxidizing and bleaching property, H_2O_2 has been widely employed in industries and clinical laboratories. Due to the immense applications of H_2O_2, there is always a need for exploring a suitable, cost-effective, sensitive H_2O_2 quantification tool. The high specify of enzyme–substrate interactions with the usually high turnover rates of biocatalysts, enzyme based biosensors

* Corresponding author. Tel.: +886 2270 17147; fax: +886 2270 25238.
E-mail address: smchen78@ms15.hinet.net (S.-M. Chen).

0039-9140/$ – see front matter © 2011 Elsevier B.V. All rights reserved.
doi:10.1016/j.talanta.2011.09.021

have attracted significant attention these days [22]. Horseradish peroxidase (HRP) is an important heme containing redox enzyme which belongs to class III (classical secretory plant peroxidases) of the plant peroxidase super family [23]. HRP contains ferriprotoporphyrin IX prosthetic group at its active centre. It has been majorly used in amperometric H_2O_2 biosensors due to its unique ability to catalyze H_2O_2 reduction process at a specific low potential via direct electron transfer [24]. Since, bare electrode lacks the ability to promote the direct electron transfer process; it necessitates exploring novel nanocomposites materials with substantial properties to augment the electron transfer phenomena. Previous literature reports shows that direct electrochemistry of HRP has been revealed at CNTs [25,26] and metal oxides such as zinc oxide (ZnO) [27], titanium dioxide (TiO_2) [28], mesoporous TiO_2 and tin oxide (SnO_2) [29], SnO_2 nanorods [30], SiO_2 nanoparticles [31], nanostructured cerium oxide (CeO_2) [32], nickel oxide nanoparticles (NiO NPs) [33], polyquaternium–manganese oxide nanosheets [34], and zirconia nanocomposites [35]. Recently, we reported the direct electrochemistry of HRP at RuO_2 nanoparticles modified GCE [36]. However, thorough view of literature reveals that no one has attempted to explore the direct electrochemistry of HRP at Bi_2O_3–MWCNT nanocomposite.

In this work, we prepared Bi_2O_3–MWCNT nanocomposite and we used it as a novel electrode material to explore the direct electrochemistry of HRP. Bi_2O_3–MWCNT nanocomposite and HRP films were modified sequentially on a GCE surface by simple drop casting method. In order to provide an outer protective coating as well as to tightly anchor the HRP molecules a thin layer of nafion (NF) coating was employed as a binder. The developed NF/HRP/Bi_2O_3–MWCNT film exhibits excellent electrocatalytic activity towards H_2O_2 with high sensitivity and selectivity. Moreover, the composite film possesses good biocompatibility and appreciable operational stability.

2. Experimental

2.1. Reagents

MWCNT with O.D. 10–15 nm, I.D. 2–6 nm and length 0.1–10 μm was obtained from Aldrich. Peroxidase, from horseradish, type VI-A was purchased from Sigma. Bismuth (III) nitrate pentahydrate, 99.9% was obtained from Wako pure chemical Industries, Ltd. Polyethylene glycol solution (PEG-4000) was purchased from Sigma–Aldrich and used as received. 5 wt% NF perfluorinated ion exchange resin was purchased from Aldrich and the required NF concentrations such as 0.25, 0.5, 0.75, 1.0 and 1.25% were prepared in definite volume of 95% pure ethanol, obtained from Shimakyu's pure chemicals. The supporting electrolyte used in this study was 0.05 M phosphate buffer solution (PBS), pH 7 prepared using 0.05 M Na_2HPO_4 and NaH_2PO_4 solutions. All the reagents used in this work were of analytical grade and all aqueous solutions were prepared using doubly distilled water. Prior to each experiment, the experimental solutions were deoxygenated with pre-purified N_2 gas for 10 min and the N_2 tube was kept above the solutions to maintain an inert atmosphere.

2.2. Apparatus

Cyclic voltammetry (CV) experiments were carried out using CHI 1205b work station. A conventional three electrode cell containing freshly prepared 0.05 M PBS (pH 7) was used for electrochemical studies. GCE with an electrode surface area of 0.079 cm^2 was used as working electrode. Pt wire with 0.5 mm diameter was used as counter electrode and all the potentials were referred with respect to standard Ag/AgCl reference electrode. Amperometric (i–t curve) measurements were performed using CHI-750 potentiostat with analytical rotator AFMSRX (PINE instruments, USA). EIM6ex ZAHNER (Kroanch, Germany) was used for electrochemical impedance spectroscopy (EIS) studies. Surface morphological studies were carried out using Hitachi S-3000 H scanning electron microscope (SEM) and Being nano-instruments CSPM 4000, atomic force microscope (AFM). Field emission scanning electron microscope (FESEM), JSM-6500F was used to investigate the surface morphology of as-prepared Bi_2O_3 nanoparticles. Energy-dispersive X-ray (EDX) spectra was recorded using HORIBA EMAX X-ACT (Model 51-ADD0009, Sensor + 24 V = 16 W, resolution at 5.9 keV = 129 eV). Powder X-ray diffraction (XRD) studies were performed in a XPERT-PRO (PANalytical B.V., The Netherlands) diffractometer using Cu Kα radiation (k = 1.54 A°). UV–visible absorption spectroscopy measurements were carried out using Hitachi U-3300 spectrophotometer.

2.3. Preparation and characterization of Bi_2O_3 nanoparticles using FESEM studies

Bi_2O_3 nanoparticles were prepared according to the procedure reported elsewhere in the literature [37]. Transparent Bi^{3+} aqueous solution was obtained by dissolving 0.05 mol $Bi(NO_3)_3$ in 30 ml 0.05 M HNO_3, to which 20 ml polyethylene glycol (PEG-4000) was added as dispersant. Then 50 ml of 4 M NaOH aqueous solution was quickly poured into this solution with vigorous stirring, which immediately leads to the formation of yellowish precipitate. The whole reaction mixture was kept at 90 °C and stirred continuously for 2 h. Then the as-produced precipitates were filtered, washed with alcohol and doubly distilled water for several times, and then dried at 60 °C in an air oven. Finally, faint yellowish Bi_2O_3 samples were obtained. Since the prepared Bi_2O_3 nanoparticles are sparingly soluble in water, we dispersed the accurately weighed quantities of Bi_2O_3 nanoparticles in DMF solution to obtain a final concentration of 1 mg ml^{-1}. The as-obtained Bi_2O_3/DMF dispersion was evenly spread on a pre-cleaned indium tin oxide electrode (ITO) surface and dried well in an air oven to evaporate the solvent molecules. The prepared Bi_2O_3 nanoparticles coated ITO electrode was used for FESEM study. The FESEM image of the Bi_2O_3 nanoparticles at 100 nm resolutions is shown in Fig. 1. The Bi_2O_3 nanoparticles possess highly porous surface morphology. Spherical shaped Bi_2O_3 nanoparticles are closely distributed throughout the film surface. The Bi_2O_3 nanoparticles are 50 nm in size. The large surface area and porous architecture of Bi_2O_3 nanoparticles can enhance the enzyme loading.

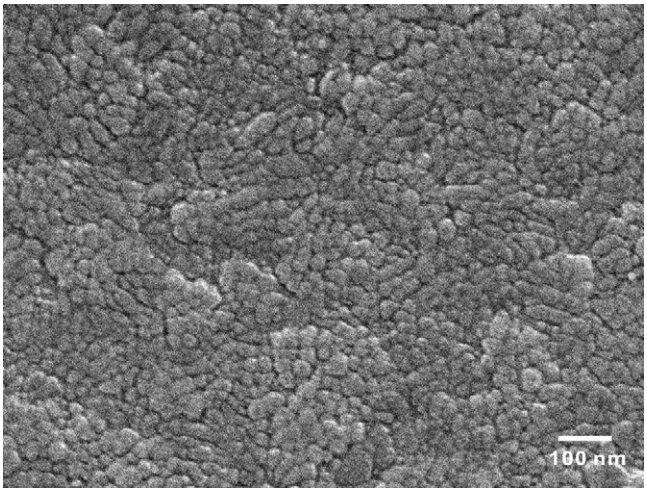

Fig. 1. FESEM image of Bi_2O_3 nanoparticles.

2.4. Preparation of Bi_2O_3–MWCNT nanocomposite

In a typical procedure, about 1 mg of as-synthesized Bi_2O_3 nanoparticles were added in to 1 ml of MWCNT/DMF solution and the whole mixture was ultrasonicated for 1 h. Thus uniform, pale blackish, homogeneous Bi_2O_3 nanoparticles/DMF dispersion was obtained. In order to explore the role of Bi_2O_3 in the nanocomposite, 1 mg ml^{-1} of MWCNT/DMF dispersion was prepared without any Bi_2O_3 nanoparticles addition. Hereafter, the terms MWCNT and Bi_2O_3–MWCNT mentioned elsewhere in this work will indicate MWCNT dispersion prepared without and with Bi_2O_3 nanoparticles.

2.5. Biosensor fabrication procedure

5 mg ml^{-1} of HRP in 0.05 M PBS (pH 7) and 1% NF in ethanol were prepared separately and stored at 4 °C. GCE surface was polished with clean Buehler polishing cloth using 0.05 μm alumina slurry and washed with doubly distilled water to remove the loosely adsorbed alumina particles. 10 μl of Bi_2O_3–MWCNT dispersion was drop casted on the clean GCE surface and dried for 30 min. The resulting Bi_2O_3–MWCNT modified GCE surface was drop casted with 10 μl of HRP solution and dried at 30 °C for 30 min. Finally, 4 μl of 1% NF solution was evenly spread on the HRP film surface and dried well at 30 °C. As reported by Zhou et al. the isoelectric point (p*I*) of HRP is 8.9, therefore HRP possess positive surface charge in pH 7 [38]. Previous study by Huang et al. provides evidence that the negative sulphonate groups of NF may bind to the positive surface charge of cytochrome *c* in pH 7 [39]. Similarly, in the present study we expect similar electrostatic interaction between the negative sulphonate groups of NF and positive surface of HRP, which may aid firm anchoring of HRP at the modified electrode surface. The prepared NF/HRP/Bi_2O_3–MWCNT/GCE was washed few times with doubly distilled water and used for further studies. For comparison studies, HRP, HRP/Bi_2O_3 and NF/HRP/MWCNT film modified electrodes were also prepared. All the modified electrodes were stored in 0.05 M PBS (pH 7) at 4 °C when not in use.

3. Results and discussion

3.1. Surface morphological characterization studies using SEM and AFM

The surface morphology of various films has been investigated using SEM studies. Fig. 2(A) shows the SEM image of Bi_2O_3 nanocrystals with variable sizes such as nanorods, nanotubes and spherical nanoparticles. In particular, Bi_2O_3 nanoparticles appear as bright spots. The rod or tube structures can be formed due to association of smaller Bi_2O_3 nanoparticles. Fig. 2(B) shows the SEM image of Bi_2O_3–MWCNT with bright Bi_2O_3 nanoparticles coated MWCNT networks. On the other hand, Fig. 2(C) shows the SEM image of MWCNTs, where several coiled MWCNT bundles were found along with few agglomerated MWCNT bundles. Fig. 2(D) shows the SEM image of NF/HRP/Bi_2O_3–MWCNT film. The large surface area of MWCNT and porous nature of Bi_2O_3 nanoparticles offers a good platform for anchoring HRP molecules. As a result more amount of HRP has been immobilized at the Bi_2O_3–MWCNT matrix. Unlike Bi_2O_3–MWCNT film surface, the NF/HRP/Bi_2O_3–MWCNT film contains slightly larger voids on its surface. However, these voids are loaded well with HRP, indicating the efficient enzyme loading.

Fig. 3(A) shows the AFM image of Bi_2O_3 nanoparticles. Several small bright spherical shaped Bi_2O_3 nanoparticles are more closely anchored throughout the film surface. The size of the Bi_2O_3 nanoparticles is between 50 and 150 nm. Few larger bright particles with 150–300 nm size were also found. The average surface roughness and root mean square roughness values are 3.09 nm and 4.14 nm, which indicated the rough surface morphology of Bi_2O_3 nanoparticles. The AFM image of Bi_2O_3–MWCNT nanocomposite is shown in Fig. 3(B), which contains both spherical shaped Bi_2O_3 nanoparticles and MWCNT. Only few bright particles are seen. No

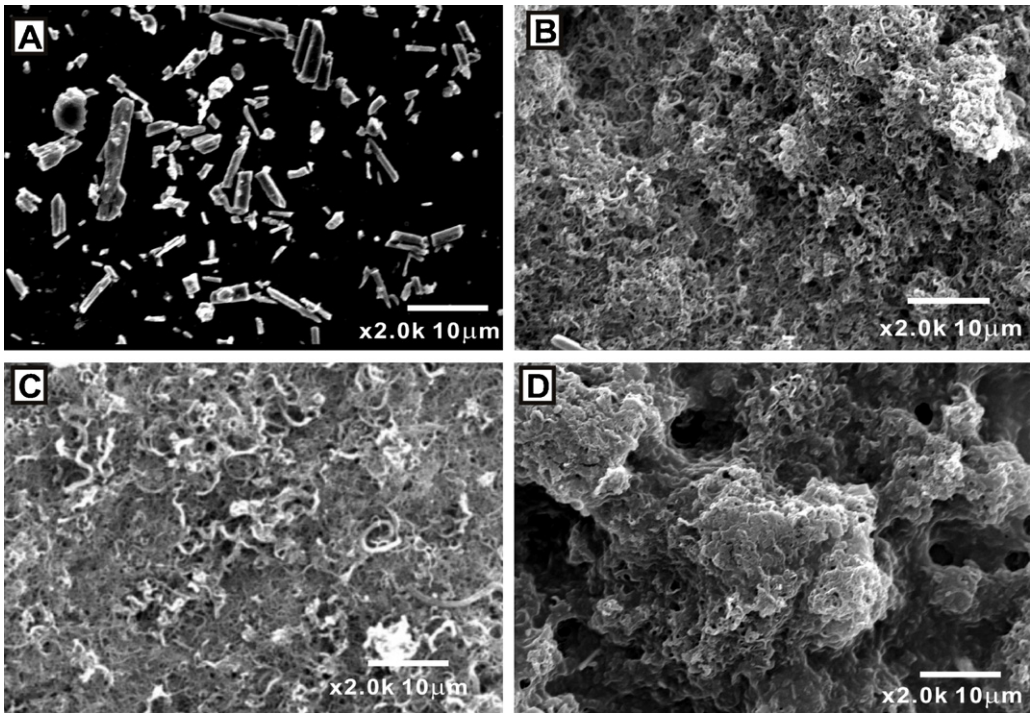

Fig. 2. SEM images of (A) Bi_2O_3 nanoparticles, (B) Bi_2O_3–MWCNT and (C) MWCNT and (D) NF/HRP/Bi_2O_3–MWCNT films.

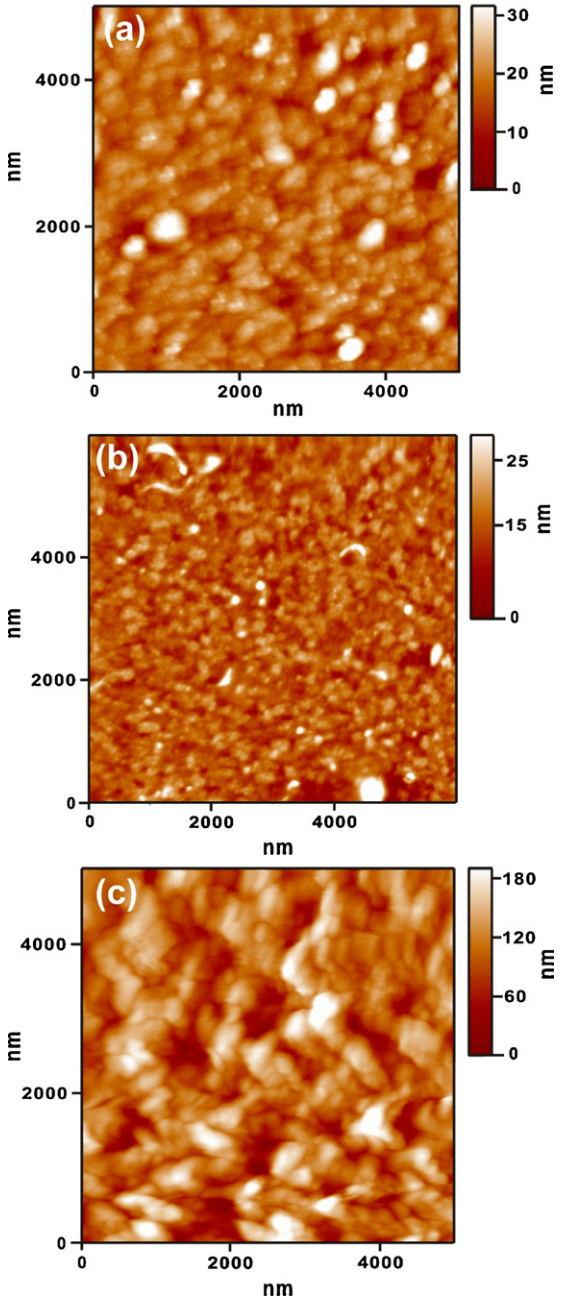

Fig. 3. AFM images of (A) Bi_2O_3 nanoparticles, (B) Bi_2O_3–MWCNT and (C) NF/HRP/Bi_2O_3–MWCNT films.

larger particles or their agglomerates were observed. The average surface roughness and root mean square roughness values of Bi_2O_3–MWCNT is 2.71 nm and 3.59 nm which shows its porous rough surface morphology. On the other hand, Fig. 3(C) shows the AFM image of HRP immobilized Bi_2O_3–MWCNT film with distinct surface morphology. HRP molecules are well immobilized at the nanocomposite matrix. Several bright spherical shaped particles are found. The AFM results are in good agreement with the SEM results, the composite film displays many voids on its surface and these voids were loaded well with HRP molecules. The average surface roughness and root mean square roughness values observed at NF/HRP/Bi_2O_3–MWCNT film is 26.3 nm and 33.1 nm, which is significantly higher than the roughness values of Bi_2O_3 nanoparticles and Bi_2O_3–MWCNT films indicating high HRP loading at the former. This could be ascribed to the large surface area and

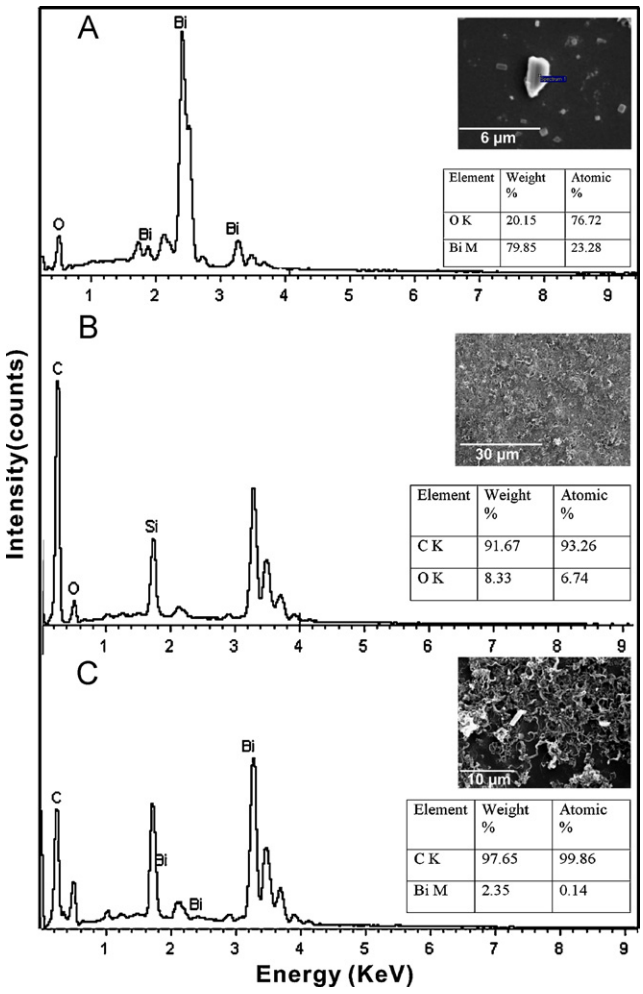

Fig. 4. EDX spectra of (A) Bi_2O_3 nanoparticles, (B) MWCNT and (C) Bi_2O_3–MWCNT films. The insets show their corresponding SEM images. The elemental composition for all the above said films with atomic and weight percentage has been given in the inset table.

highly porous surface morphology of MWCNT and Bi_2O_3 nanoparticles.

3.2. EDX spectra analysis

EDX spectra results have been used to confirm the formation of Bi_2O_3–MWCNT. The EDX spectra of Bi_2O_3 nanoparticles presented in Fig. 4(A) exhibits well defined peaks for Bi and O elements, confirming the presence of Bi_2O_3 nanoparticles. The corresponding SEM image is shown in Fig. 4(A) inset, which depicts the as-synthesized Bi_2O_3 nanocrystals with variable sizes. From the atomic and weight percentage values, it is clear that Bi_2O_3 nanoparticles are richer with the elements Bi and O. Where as, the EDX spectra of MWCNT in Fig. 4(B) shows intense peaks for the elements C and O indicating the presence of various carbon and oxygen containing functional groups at the MWCNT surface. The weight and atomic percentage values for the elements C and O are 91.67, 93.26% and 8.33, 6.74%, respectively. The SEM image of MWCNT film is also provided in the inset of Fig. 4(B). Interestingly, the EDX spectra of Bi_2O_3–MWCNT nanocomposite shown in Fig. 4(C) exhibits both Bi and C peaks, indicating the presence of Bi_2O_3 and MWCNT in the nanocomposite. The formation of Bi_2O_3–MWCNT has also been confirmed from the atomic, weight percentage values and the SEM image of Bi_2O_3–MWCNT film given in the inset of Fig. 4(C).

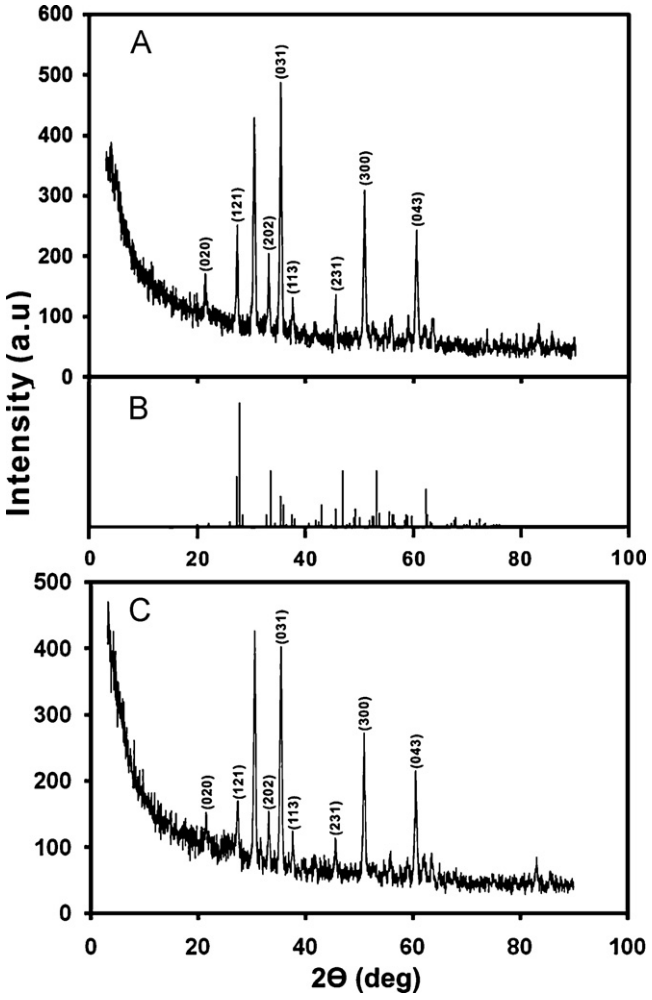

Fig. 5. (A) Powder XRD pattern of as-synthesized α-Bi_2O_3 nanoparticles (B) standard powder XRD pattern of α-Bi_2O_3 (PDF # 710465) and (C) powder XRD pattern of Bi_2O_3–MWCNT nanocomposite.

3.3. XRD studies

Fig. 5(A) shows the powder XRD pattern of α-Bi_2O_3 nanoparticles synthesized in this work. Li reported a mixture of two distinct crystal phases such as monoclinic α-Bi_2O_3 and triclinic ω-Bi_2O_3 phase by adapting the solution based approach [37]. However, in our case majority of the peak positions and the corresponding 2θ angles are consistent with the standard powder XRD pattern of monoclinic, α-Bi_2O_3 nanoparticles (PDF # 710465) shown in Fig. 5(B). Thus the Bi_2O_3 nanoparticles synthesized in this work are α-Bi_2O_3 and it has a monoclinic symmetry with a space group of $P2_1/c(14)$. The cell parameters are $a = 5.849$, $b = 8.164$, and $c = 7.510$, respectively. Similarly, as shown in Fig. 5(C) the XRD pattern of Bi_2O_3–MWCNT nanocomposite also exhibits identical peaks at same 2θ values with similar intensities as that of α-Bi_2O_3, which confirmed the presence of Bi_2O_3 in the nanocomposite.

3.4. Investigation of direct electrochemistry of HRP

The direct electrochemistry of HRP was investigated at Bi_2O_3–MWCNT film modified GCE using cyclic voltammetry. Fig. 6 shows the cyclic voltammograms obtained at various films modified GCEs in 0.05 M PBS (pH 7). As shown by curves (a) and (b), no obvious redox peaks were observed at HRP/GCE and HRP/Bi_2O_3/GCE in the potential range between 0.2 and −0.7 V. Thus no apparent electron transfer process occurs at the unmodified and

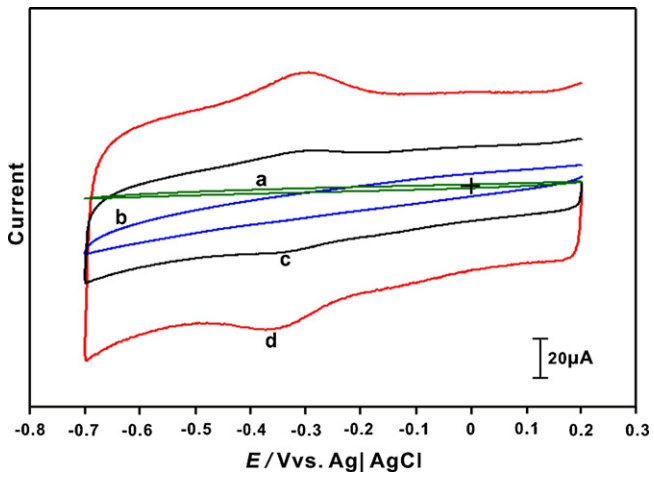

Fig. 6. Cyclic voltammograms obtained at (a) HRP, (b) HRP/Bi_2O_3 and (c) NF/HRP/MWCNT and (d) NF/HRP/Bi_2O_3–MWCNT film modified GCEs in N_2 saturated 0.05 M PBS (pH 7) at the scan rate of 50 mV s^{-1}.

HRP/Bi_2O_3 modified GCEs, ascribed to the poor electrical contact between the prosthetic group of HRP and these electrode surfaces. In contrast, as shown in curve (c), NF/HRP/MWCNT/GCE shows well defined redox peaks at a formal potential ($E^{0\prime}$) of −0.324 V. This represents the unique ability of MWCNT to triumph the direct electron transfer of HRP as better electrical communication has been established via MWCNT. Compared with NF/HRP/MWCNT/GCE, enhanced redox peaks at an $E^{0\prime}$ value of −0.326 V is observed at NF/HRP/Bi_2O_3–MWCNT/GCE which indicates the fast electron transfer process at the later (see curve (d)). The $E^{0\prime}$ value (−0.326 V) of HRP reported at NF/HRP/Bi_2O_3–MWCNT film is close to the $E^{0\prime}$ value (−0.328 V) of HRP reported at MWCNT/alumina-coated silica nanocomposite modified GCE vs. Ag/AgCl reference electrode [40]. The electron transfer process occurring at the nanocomposite film matrix thus belongs to the $Fe^{(III/II)}$ redox electrochemical process of the immobilized HRP.

3.5. Effect of scan rate and pH

Fig. 7 shows the cyclic voltammograms obtained at NF/HRP/Bi_2O_3–MWCNT/GCE in N_2 saturated 0.05 M PBS (pH 7) at different scan rates. The peak currents (I_{pa} and I_{pc}) vs. scan rates plot shown in Fig. 7 inset exhibits a linear relationship with $R^2 = 0.999$ and 0.9997, respectively. Both I_{pa} and I_{pc} increased linearly with increase in scan rates between 50 and 500 mV s^{-1}, thus the $Fe^{(III/II)}$ redox process occurring at NF/HRP/Bi_2O_3–MWCNT/GCE is surface-confined. The surface coverage (Γ) value of HRP immobilized at NF/HRP/Bi_2O_3–MWCNT/GCE has been calculated using the formula given in Eq. (1)

$$\Gamma = \frac{Q}{nFA} \quad (1)$$

where Q is the charge, n is the number of electrons transferred, F is the Faraday current and A is the electrode area. Where, the number of electrons transferred is 1 for $Fe^{(III/II)}$ redox reaction of HRP. The Γ value of HRP immobilized at NF/HRP/Bi_2O_3–MWCNT/GCE is calculated to be about 2.52×10^{-10} mol cm^{-2}, which is higher than the Γ values of HRP reported at NF-HRP-CNT/GC ($\Gamma = 1.90 \pm 0.44 \times 10^{-12}$ mol cm^{-2}) [41], and other HRP modified electrodes [42–44]. The higher Γ value of HRP reported in this work can be ascribed to the porous nature of Bi_2O_3 nanoparticles and large surface area of MWCNT which enables high enzyme loading.

As shown in Fig. S1 well-defined quasi-reversible redox peaks corresponding to $Fe^{(III/II)}$ redox process of HRP was observed at NF/HRP/Bi_2O_3–MWCNT/GCE in the pH range between 4 and 11.

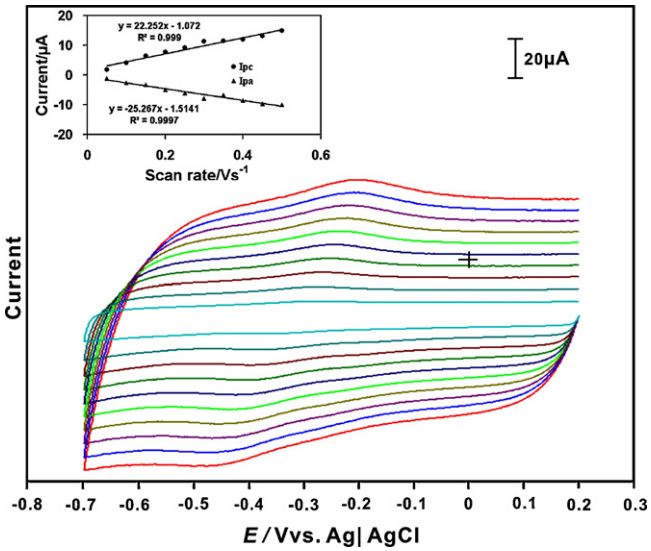

Fig. 7. Cyclic voltammograms obtained at NF/HRP/Bi_2O_3–MWCNT film modified GCE in N_2 saturated 0.05 M PBS (pH 7) at different scan rates. The scan rates from inner to outer are between 50, 100, 150, 200, 250, 300, 350, 400, 450, and 500 mV s^{-1}. The inset shows the linear dependence plot of peak currents (I_{pa} and I_{pc}) vs. scan rates/V s^{-1}.

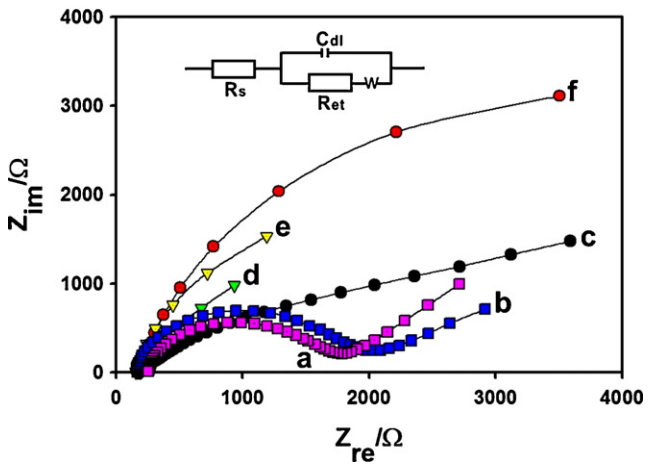

Fig. 8. (a) EIS of (a) bare, (b) HRP, (c) Bi_2O_3–MWCNT, (d) MWCNT, (e) NF/HRP/MWCNT, and (f) NF/HRP/Bi_2O_3–MWCNT film modified GCEs in 0.05 M PBS (pH 7) containing 5 mM $Fe(CN)_6^{3-}$/$Fe(CN)_6^{4-}$. Amplitude: 5 mV, frequency: 100 mHz–100 kHz. EIS data obtained at all modified electrodes were fitted using the Randles equivalence circuit given in the inset.

This shows the stability of the composite film in wide pH range. In particular, well defined redox peaks with enhanced peak currents were observed in pH 7 as the HRP retains its bioactivity in neutral pH. Fig. S1 inset, shows the linear dependence of E_{pa}, E_{pc} and $E^{0\prime}$ of the redox couple of HRP with pH. The $E^{0\prime}$ values showed a negative shift with increase in pH with a slope value of 41.8 mV pH^{-1}, respectively. This slope value is close to the theoretical slope value of 59 mV pH^{-1} for equal number of electron and proton transfer process. The slope value of HRP reported in this study is also closer to the slope of 37.8 mV pH^{-1} reported at HRP/DDAB–HIMIMPF_6 film [42]. As explained in previous literature, the reasons for the smaller slope values might be ascribed to the protonation states of trans ligands to the heme iron and amino acids around the heme, or because of the protonation of the water molecule coordinated to the central iron [45,46].

3.6. Biocompatibility study using UV–vis absorption spectroscopy

UV–vis absorption spectra can be used as an effective tool to probe whether the heme proteins retain their native structure at the immobilization matrix. This kind of information can be explicated from the exact location and from the shift in position of the soret absorption band of heme prosthetic group. So we utilized UV–vis absorption spectroscopy as a handy tool to probe whether HRP retains its native structure at Bi_2O_3–MWCNT nanocomposite. Fig. S2 shows the UV–visible absorption spectra of NF/HRP/Bi_2O_3–MWCNT film. A broad absorption band at 400 nm has been observed for NF/HRP/Bi_2O_3–MWCNT film which is close to the soret band of HRP casted films (404 nm and 406 nm) reported before [47]. Since HRP retains its soret band without any notable wavelength shift, the nanocomposite matrix should be highly biocompatible for the immobilized HRP.

3.7. EIS studies at various film modified GCEs

Fig. 8 shows the real and imaginary parts of the impedance spectra represented as Nyquist plots (Z_{im} vs. Z_{re}) for various film modified GCEs in 0.05 M PBS (pH 7) containing 5 mM $Fe(CN)_6^{3-/4-}$. In Fig. 8, curve (a) displays well defined semicircle at unmodified GCE which indicates the sluggish electron transfer process. Compared with bare GCE, HRP modified GCE shown in curve (b) exhibits slightly larger semicircle than bare GCE. The increase in the electron transfer resistance (R_{et}) value at HRP/GCE is due to the inaccessibility of the heme redox entre since it is covered by thick polypeptide layer. Unlike the unmodified and HRP modified GCEs, Bi_2O_3–MWCNT and MWCNT modified GCEs does not show any semicircles instead they exhibited straight lines representing the diffusion-limited electrochemical process (see curves (c) and (d)). The decrease in R_{et} values at Bi_2O_3–MWCNT and MWCNT modified GCE surfaces showed the excellent electron transfer ability of MWCNT. Similarly as shown in curves (e) and (f), NF/HRP/MWCNT and NF/HRP/Bi_2O_3–MWCNT film modified GCEs showed slightly bent lines with increased R_{et} values which can be ascribed to the non-conductive properties of HRP which hinder the electron transfer of the electrochemical probe [48]. Thus EIS results confirmed the immobilization of HRP at the nanocomposite.

3.8. Electrocatalytic H_2O_2 reduction studies

We investigated the electrocatalytic activity of the HRP immobilized nanocomposite film towards H_2O_2 in 0.05 M PBS (pH 7). Fig. 9(a) shows the cyclic voltamograms obtained at NF/HRP/Bi_2O_3–MWCNT/GCE in the absence of H_2O_2. While the curves (b-i) represents the cyclic voltammograms obtained at the composite film in presence of various H_2O_2 concentrations. An enhanced catalytic reduction peak was observed at an I_{pc} of −0.18 V for 3.6 μM H_2O_2 (curve b). Since then, the cathodic peak currents increased gradually with increase in H_2O_2 concentrations while anodic peak currents decreased ((Fig. 9(c–i)). Where, both the increase in peak current and decrease in over potential are considered as electrocatalysis [49]. In contrast, bare GCE exhibits ill-defined peak at −0.6 V for 222.2 μM H_2O_2, which shows its poor electrocatalytic activity towards H_2O_2 (see curve (a′) in Fig. 9). Compared with the H_2O_2 reduction potential (−0.6 V) of bare GCE, composite film modified GCE exhibits enhanced reduction peak at much lower potential (−0.23 V), which indicates that composite film has reduced the over potential by 370 mV. The good electrocatalytic activity can be ascribed to the synergistic effect of the nanocomposite towards H_2O_2. The NF/HRP/Bi_2O_3–MWCNT/GCE exhibits promising electrocatalytic activity towards H_2O_2 in the linear concentration range between 19.2 and 222.1 μM H_2O_2 with a sensitivity of 1.62 μA mM^{-1} cm^{-2}. The linear regression equation is I (μA) = 0.1282C (μM) + 2.2514, R^2 = 0.9845.

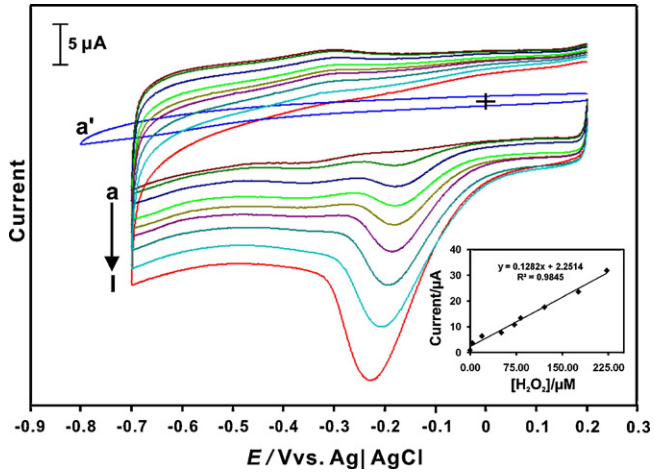

Fig. 9. Cyclic voltammograms obtained at NF/HRP/Bi_2O_3–MWCNT/GCE at the scan rate of 50 mV s^{-1} in the (a) absence and presence of (b) 3.6 (c) 19.2, (d) 50.9, (e) 72.0, (f) 82.2, (g) 121.0, (h) 176.0, and (i) 222.2 µM H_2O_2, (a′) bare/GCE in the presence of 222.2 µM H_2O_2. Supporting electrolyte: N_2 saturated 0.05 M PBS (pH 7). Inset is the plot of cathodic peak current vs. [H_2O_2].

We investigated the influence of NF coating on the electrocatalytic activity of HRP using CV studies. The NF concentrations used were 0.25, 0.5, 0.75, 1.0 and 1.25%, respectively. Cyclic voltammograms were obtained at the biosensors fabricated using the above mentioned NF concentrations in N_2 saturated 0.05 M PBS (pH 7) containing 100 µM H_2O_2 at the scan rate of 50 mV s^{-1} (CVs not shown). From the as-obtained cyclic voltammograms, the electrocatalytic reduction current has been calculated and plotted against various NF concentrations as shown in Fig. S3. It is clear that, the response current increased slightly for 0.25 and 0.5% NF, where as it decreased for 0.75 and 1.25% NF. However, maximum response current was observed at the biosensor fabricated with 1% NF, so we used this optimized NF concentration for all our electrocatalytic experiments.

We also attempted to compare the electrocatalytic activity of various modified electrodes. In Fig. 10, curves (a–d) show the electrocatalytic responses obtained at various modified electrodes in the presence of 222.1 µM H_2O_2. Among all the investigated electrodes, as shown in curve (d), NF/HRP/Bi_2O_3–MWCNT/GCE shows enhanced electrocatalytic reduction peak at much low

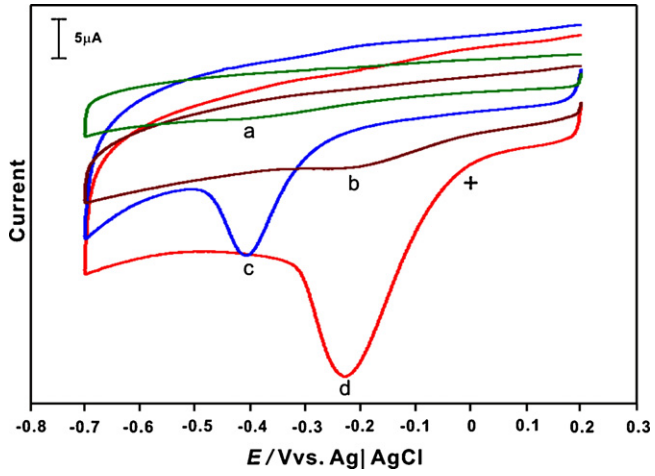

Fig. 10. Cyclic voltammograms obtained at (a) MWCNT, (b) NF/HRP/MWCNT, (c) Bi_2O_3–MWCNT, and (d) NF/HRP/Bi_2O_3–MWCNT/GCEs at the scan rate of 50 mV s^{-1} in the presence of 222.1 µM H_2O_2. Supporting electrolyte is N_2 saturated 0.05 M PBS (pH 7).

reduction potential of −0.223 V. Comparatively, as shown in curves (a and b) MWCNT, and NF/HRP/MWCNT/GCE displayed small shoulder peaks at −0.412 V and −0.223 V, respectively. While as shown in curve (c), Bi_2O_3–MWCNT modified electrode exhibits an enhanced reduction peak at −0.339. It is noteworthy that compared with MWCNT and Bi_2O_3–MWCNT films, the NF/HRP/Bi_2O_3–MWCNT/GCE considerably decreased the overpotential by 189 and 176 mV respectively. Moreover, the electrocatalytic current observed at the composite film is several folds higher than the electrocatalytic current observed at NF/HRP/MWCNT/GCE. The excellent electrocatalytic H_2O_2 reduction results achieved at NF/HRP/Bi_2O_3–MWCNT film corroborates its low potential H_2O_2 sensing ability, which could be ascribed to the good biocompatibility of the Bi_2O_3–MWCNT nanocomposite for HRP and synergistic effect of the Bi_2O_3–MWCNTs for H_2O_2.

3.9. Amperometric *i–t* curve studies

During the amperometric experiments the electrode potential was held at −0.3 V and the N_2 saturated 0.05 M PBS (pH 7) was continuously stirred at 900 rpm. For every 50 s, aliquots of H_2O_2 were successively injected into the supporting electrolyte solution. Fig. 11(A) shows the amperometric *i–t* response obtained at NF/HRP/Bi_2O_3–MWCNT rotating GCE upon various H_2O_2 concentration additions. The composite film exhibits rapid, well-defined amperometric response towards various H_2O_2 concentration additions. The response time of the NF/HRP/Bi_2O_3–MWCNT composite film towards H_2O_2 was 5 s, validating the rapid catalytic reduction process occurring at the composite film surface. The amperometric response current increased linearly with increase in H_2O_2 concentrations between 6.63 mM and 30.12 mM H_2O_2 (Fig. 11(A) inset). From the calibration plot, the linear concentration range, correlation coefficient and the sensitivity values are calculated as 8.34–28.88 mM H_2O_2, 0.9743 and 26.54 µA mM^{-1} cm^{-2}, respectively. The linear regression equation is I (µA) = 6.3698C (µM) + 7.0994, R^2 = 0.9743. The essential analytical parameters such as applied potential, sensitivity, response time and linear concentration range of the proposed NF/HRP/Bi_2O_3–MWCNT film have been compared with other HRP based biosensors available in literature [50–52,26,53–55,36] as exemplified in Table 1. The proposed biosensor detects H_2O_2 at low operating potential (−0.3 V vs. Ag/AgCl), with high sensitivity, short response time in wide linear concentration range. The satisfactory amperometric H_2O_2 determination results achieved at the NF/HRP/Bi_2O_3–MWCNT film in this study could be attributed to the good affinity of the immobilized HRP for H_2O_2 and the efficient immobilization of HRP at Bi_2O_3–MWCNT matrix.

It is well known that the biological fluids contain H_2O_2 along with ascorbic acid (AA), uric acid (UA), and dopamine (DA). Therefore, the selectivity of the developed NF/HRP/Bi_2O_3–MWCNT composite film is mandatory and it was evaluated in the presence of the above said interfering species in same 0.05 M PBS (pH 7). In Fig. 11(B), NF/HRP/Bi_2O_3–MWCNT film shows rapid, well defined amperometric response towards 100 µM H_2O_2. In contrast, no notable amperometric signals were observed for each 100 µM of UA, AA and DA concentration additions. The selectivity results thus confirmed that the proposed HRP biosensor is highly selective and it successfully overcomes the matrix effect caused by the common interferences. The good selectivity of the composite film could be ascribed to the anti-interference ability of the outer NF layer [56].

The operational stability of NF/HRP/Bi_2O_3–MWCNT modified rotating disc electrode was examined by amperometry. Fig. S4 shows the amperometric *i–t* response observed at NF/HRP/Bi_2O_3–MWCNT film for 100 µM H_2O_2. Under hydronamic rotating conditions (900 rpm), the composite film exhibits well defined amperometric response for 100 µM H_2O_2 and the response

Table 1
Comparison of electroanalytical values obtained in this work for H_2O_2 quantification with other HRP based electrodes reported in literature.

Electrode	Applied potential (V)	Sensitivity	[a]Response time (s)	Linear range (mM)	Ref.
[b]HRP–AuNPs–SF/GCE	−0.6 vs. SCE	Not available	<8	0.01–1.8	[50]
[c]HRP/HNTs/Chi	−0.40 vs. SCE	12.25 μA mM^{-1}	5	0.0026–0.075	[51]
[d]Self-assembled HRP/laponite/Chit/GCE	−0.45 vs. SCE	19.7 ± 0.5 mA M^{-1} cm^{-2-}	10	0.029–1.4	[52]
[e]HRP–SWCNTs–CTAB	−0.40 vs. SCE	0.133 μA mM^{-1}	<4	0.0123–0.145	[26]
HRP/Au colloid/cysteamine-modified electrode	−0.3 vs. SCE	Not available	<15	0.0014–9.2	[53]
Sol–gel/chitosan modified HRP electrode	−0.1 vs. SCE	14.86 μA mM^{-1}	<10	0.25–3.4	[54]
[f]MB–SiO_2/HRP	−0.3 vs. SCE	Not available	<20	0.01–1.2	[55]
[g]HRP/Chi-GAD/RuNPs	−0.3 vs. Ag/AgCl	0.798 μA mM^{-1} cm^{-2}	5	5.09–15	[36]
NF/HRP/Bi_2O_3–MWCNT/GCE	−0.3 vs. Ag/AgCl	26.54 μA mM^{-1} cm^{-2}	5	8.34–28.88	This work

[a] Response time mentioned here is the time required for the biosensor to reach 90 (or) 95 (%) of the maximum steady-state response.
[b] HRP immobilized at gold nanoparticles-silk fibroin modified GCE.
[c] HRP immobilized at halloysitenanotubes/chitosan modified GCE.
[d] HRP self-assembled at laponite/chitosan modified GCE.
[e] HRP incorporated single walled carbon nanotubes-cetylramethylammonium bromide nanocomposite film modified GCE.
[f] Silica–methylene blue/gelatin/HRP film modified GCE.
[g] HRP immobilized at ruthenium oxide nanoparticles modified GCE via chitosan/glutaraldehyde crosslinking.

current was highly stable up to 5000s. No notable decrease in the response current was observed even after 5000 s which shows the good operational stability of the composite film. The reason for such a long-time operational stability can be ascribed to the good biocompatibility and appreciable stability of the HRP immobilized Bi_2O_3–MWCNT nanocomposite.

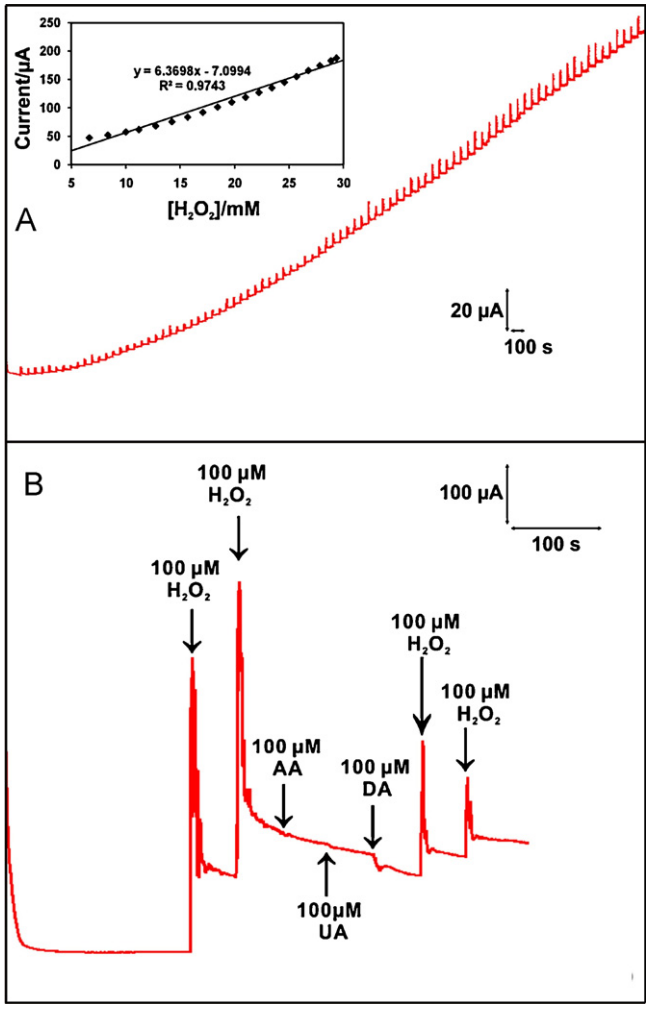

Fig. 11. Amperometric *i–t* responses at NF/HRP/Bi_2O_3–MWCNT film modified rotating disc GCE upon successive additions of 6.63–30.12 mM H_2O_2. The inset is the plot of linear response current vs. [H_2O_2] = 8.34–28.88 mM. (B) Amperometric *i–t* responses at NF/HRP/Bi_2O_3–MWCNT film modified rotating GCE for the successive 100 μM of H_2O_2, AA, UA, and DA concentration additions. Applied potential: −0.3 V; Rotation rate: 900 rpm. Supporting electrolyte: continuously stirred N_2 saturated 0.05 M PBS (pH 7).

3.10. Repeatability, reproducibility and storage stability studies

The repeatability and reproducibility of the biosensor was examined by CV studies. The potential range used for CV studies is between 0.2 and −0.7 V and the supporting electrolyte used was N_2 saturated 0.05 M PBS (pH 7). Repetitive CV measurements were carried out at the NF/HRP/Bi_2O_3–MWCNT film modified GCE at the scan rate of 50 mV s^{-1} towards each 100 μM H_2O_2 additions. The supporting electrolyte solution has been renewed for each measurement before the addition of target analyte. The % relative standard deviation (R.S.D.) for five successive 100 μM H_2O_2 measurements at NF/HRP/Bi_2O_3–MWCNT/GCE is 2.8% which shows the acceptable repeatability of the proposed method. The R.S.D. for 100 μM H_2O_2 response at five different NF/HRP/Bi_2O_3–MWCNT modified GCEs is 2.82%, validating the good reproducibility of the proposed biosensor.

We also investigated the storage stability of the proposed HRP based biosensor using CV studies. NF/HRP/Bi_2O_3–MWCNT film modified GCE was stored in 0.05 M PBS (pH 7) at 4 °C, the peak current (I_{pc}) and the response current observed at the biosensor both in the absence and presence of 100 μM H_2O_2 was monitored regularly for one week. After four days, the biosensor retained 94.6% peak current and in the consecutive days a slight decrease in peak current was observed, which shows the reasonable storage stability of the proposed biosensor. Throughout the one week storage period, the biosensor exhibits well defined catalytic response towards 100 μM H_2O_2 and it retains 94.4% response current even after one week, which revealed that HRP has been well immobilized and it retains its biocatalytic activity at the nanocomposite film matrix.

4. Conclusions

We report a simple two-step solution phase approach to prepare Bi_2O_3–MWCNT nanocomposite. In the first step, α-Bi_2O_3 nanoparticles were precipitated from $Bi(NO_3)_3$ precursor solution using PEG as the dispersant under strong alkaline conditions. In the second step the as-synthesized crystalline α-Bi_2O_3 nanoparticles were dispersed with MWCNTs in a DMF solution by simple ultrasonication treatment to form well-dispersed, homogeneous Bi_2O_3–MWCNT nanocomposite. The formation of Bi_2O_3–MWCNT was confirmed by surface morphological studies such as SEM, AFM, powder XRD and EDX spectra. The direct electrochemistry of HRP was revealed at the Bi_2O_3–MWCNT/GCE surface via cyclic voltammetry. The NF/HRP/Bi_2O_3–MWCNT sensing platform exhibits excellent

electrocatalytic response towards H_2O_2 in wide range with high sensitivity and it considerably decreased the over potential for H_2O_2 reduction. The nanocomposite sensing platform offers efficient enzyme loading and it facilitates fast electron transfer and it provides remarkable operational stability and selectivity with good biocompatibility. The preset work may thus encourage the exploitation of MWCNT–metal oxide nanocomposites as potent immobilization matrices for probing the direct electrochemistry of heme group containing redox enzymes.

Acknowledgement

This work was supported by the National Science Council and the Ministry of Education of Taiwan (Republic of China).

Appendix A. Supplementary data

Supplementary data associated with this article can be found, in the online version, at doi:10.1016/j.talanta.2011.09.021.

References

[1] L. Agui, P.Y. Sedeno, J.M. Pingarron, Anal. Chim. Acta 622 (2008) 11–47.
[2] P.A. Prakash, U. Yogeswaran, S.M. Chen, Talanta 78 (2009) 1414–1421.
[3] A. Mikolajczuk, A. Borodzinski, L. Stobinski, P. Kedzierzawski, B. Lesiak, L. Kover, J. Toth, H.M. Lin, Phys. Status Solidi B 247 (2010) 3063–3067.
[4] T. Sawatsuk, A. Chindaduang, C.S. Kung, S. Pratontep, G. Tumcharern, Diam. Relat. Mater. 18 (2009) 524–527.
[5] S. Campidelli, C. Klumpp, A. Bianco, D.M. Guldi, M. Prato, J. Phys. Org. Chem. 19 (2006) 531–539.
[6] U. Yogeswaran, S. Thiagarajan, S.M. Chen, Anal. Biochem. 365 (2007) 122–131.
[7] W.D. Zhang, B. Xu, L.C. Jiang, J. Mater. Chem. 20 (2010) 6383–6391.
[8] U. Yogeswaran, S.M. Chen, Sens. Actuators B 130 (2008) 739–749.
[9] Y. Umasankar, A.P. Periasamy, S.M. Chen, Anal. Biochem. 411 (2011) 71–79.
[10] M.Md. Rahman, A.J.S. Ahammad, J.H. Jin, S.J. Ahn, J.J. Lee, Sensors 10 (2010) 4855–4886.
[11] A. Arvinte, A.C. Westermann, A.M. Sesay, V. Virtanen, Sens. Actuators B 150 (2010) 756–763.
[12] Z. Fan, J. Chen, M. Wang, K. Cui, H. Zhou, Y. Kuang, Diam. Relat. Mater. 15 (2006) 1478–1483.
[13] Y. Zhang, X. Sun, L. Pan, H. Li, Z. Sun, C. Sun, B.K. Tay, Solid State Ionics 180 (2009) 1525–1528.
[14] A. Goyal, A.L.M. Reddy, P.M. Ajayan, Small 7 (2011) 1709–1713.
[15] X. Chen, S. Chen, W. Huang, J. Zheng, Z. Li, Electrochim. Acta 54 (2009) 7370–7373.
[16] M. Khairy, R.O. Kadara, D.K. Kampouris, C.E. Banks, Electroanalysis 22 (2010) 1455–1459.
[17] M. Zidan, T.W. Tee, A.H. Abdullah, Z. Zainal, G.J. Kheng, Int. J. Electrochem. Sci. 6 (2011) 279–288.
[18] S. Taufik, N.A. Yusof, T.W. Tee, I. Ramli, Int. J. Electrochem. Sci. 6 (2011) 1880–1891.
[19] S.N. Ding, D. Shan, H.G. Xue, S. Cosnier, Bioelectrochemistry 79 (2010) 218–222.
[20] D. Shan, J. Zhang, H.G. Xue, Y.C. Zhang, S. Cosnier, S.N. Ding, Biosens. Bioelectron. 24 (2009) 3671–3676.
[21] R.J. Weston, Food Chem. 71 (2000) 235–239.
[22] M.I. Prodromidis, M.I. Karayannis, Electroanalysis 14 (2002) 241–261.
[23] N.C. Veitch, Phytochemistry 65 (2004) 249–259.
[24] S.V. Dzyadevych, V.N. Arkhypova, A.P. Soldatkin, A.V. Elskaya, C. Martelet, N. Jaffrezic-Renault, ITBM–RBM 29 (2008) 171.
[25] Y. Yang, G. Yang, Y. Huang, H. Bai, X. Lu, Colloids Surf. A 340 (2009) 50–55.
[26] S. Wang, F. Xie, G. Liu, Talanta 77 (2009) 1343–1350.
[27] C. Xiang, Y. Zou, L.X. Sun, F. Xu, Sens. Actuators B 136 (2009) 158–162.
[28] Y. Wang, X. Ma, Y. Wen, Y. Xing, Z. Zhang, H. Yang, Biosens. Bioelectron. 25 (2010) 2442–2446.
[29] Y. Astuti, E. Topoglidis, A.G. Cass, J.R. Durrant, Anal. Chim. Acta 648 (2009) 2–6.
[30] J. Liu, Y. Li, X. Huang, Z. Zhu, Nanoscale Res. Lett. 5 (2010) 1177–1181.
[31] P. He, N. Hu, Electroanalysis 16 (2004) 1122.
[32] A.A. Ansari, P.R. Solanki, B.D. Malhotra, J. Biotechnol. 142 (2009) 179–184.
[33] A. Mohammadi, A.B. Moghaddam, M. Kazemzad, R. Dinarvand, J. Badraghi, Mater. Sci. Eng. C 29 (2009) 1752–1758.
[34] X. Yang, X. Chen, X. Zhang, W. Yang, D.G. Evans, Sens. Actuators B 134 (2008) 182–188.
[35] S. Zong, Y. Cao, Y. Zhou, H. Ju, Langmuir 22 (2006) 8915–8919.
[36] A.P. Periasamy, S.W. Ting, S.M. Chen, Int. J. Electrochem. Sci. 6 (2011) 2688–2709.
[37] W. Li, Mater. Chem. Phys. 99 (2006) 174–180.
[38] Y. Zhou, N. Hu, Y. Zeng, J.F. Rusling, Langmuir 18 (2002) 211–219.
[39] Q. Huang, Z. Lu, J.F. Rusling, Langmuir 12 (1996) 5472–5480.
[40] J.L. Huang, Y.C. Tsai, Sens. Actuators B 140 (2009) 267–272.
[41] Y. Yin, Y. Lu, P. Wu, C. Cai, Sensors 5 (2005) 220–234.
[42] Y. Xu, C. Hu, S. Hu, Anal. Chim. Acta 663 (2010) 19–26.
[43] J.Z. Xu, J.J. Zhu, Q. Wu, Z. Hu, H.Y. Chen, Electroanalysis 15 (2003) 219–224.
[44] J.S. Long, D.S. Silvester, G.G. Wildgoose, A.E. Surkus, G. Flechsig, R.G. Compton, Bioelectrochemistry 74 (2008) 183–187.
[45] Y.X. Sun, J.T. Zhang, S.W. Huang, S.F. Wang, Sens. Actuators B 124 (2007) 494–500.
[46] I. Yamazaki, T. Araiso, Y. Hayashi, H. Yamada, R. Makino, Adv. Biophys. 11 (1978) 249–281.
[47] X. Chen, X. Peng, J. Kong, J. Deng, J. Electroanal. Chem. 480 (2000) 26–33.
[48] N. Tang, J. Zheng, Q. Sheng, H. Zhang, R. Liu, Analyst 136 (2011) 781–786.
[49] C.P. Andrieux, O. Haas, J.M. Savgant, J. Am. Chem. Soc. 108 (1986) 8175–8182.
[50] H. Yin, S. Ai, W. Shi, L. Zhu, Sens. Actuators B 137 (2009) 747–753.
[51] X. Sun, Y. Zhang, H. Shen, N. Jia, Electrochim. Acta 56 (2010) 700–705.
[52] D. Shan, Q.B. Li, S.N. Ding, J.Q. Xu, S. Cosnier, H.G. Xue, Biosens. Bioelectron. 26 (2010) 536–541.
[53] X. Yi, J.H. Xian, C.H. Yuan, Anal. Biochem. 278 (2000) 22–28.
[54] Y. Miao, S.N. Tan, Anal. Chim. Acta 437 (2001) 87–93.
[55] H. Yao, N. Li, S. Xu, J.Z. Xu, J.J. Zhu, H.Y. Chen, Biosens. Bioelectron. 21 (2005) 372–377.
[56] F.O. Brown, J.P. Lowry, Analyst 128 (2003) 700–705.